J. Fluid Mech. (2011), *vol.* 687, *pp.* 595–605.
doi:10.1017/jfm.2011.402

Magnetohydrodynamic convectons

David Lo Jacono[1,2]†, Alain Bergeon[1,2] and Edgar Knobloch[3]

[1] Université de Toulouse; INPT, UPS; IMFT (Institut de Mécanique des Fluides de Toulouse), Allée Camille Soula, F-31400 Toulouse, France

[2] CNRS; IMFT; F-31400 Toulouse, France

[3] Department of Physics, University of California, Berkeley CA 94720, USA

(Received 12 April 2011; revised 8 September 2011; accepted 19 September 2011)

Numerical continuation is used to compute branches of spatially localized structures in convection in an imposed vertical magnetic field. In periodic domains with finite spatial period, these branches exhibit slanted snaking and consist of localized states of even and odd parity. The properties of these states are analysed and related to existing asymptotic approaches valid either at small amplitude (Cox and Matthews, *Physica* D, vol. 149, 2001, p. 210), or in the limit of small magnetic diffusivity (Dawes, *J. Fluid Mech.*, vol. 570, 2007, p. 385). The transition to standard snaking with increasing domain size is explored.

Key words: bifurcation, magneto convection, pattern formation

1. Introduction

Convectons are spatially localized regions of convection embedded in a quiescent background. States of this type were found in numerical studies of magnetoconvection, i.e. convection in an imposed vertical magnetic field, in both two (Blanchflower 1999) and three spatial dimensions (Blanchflower & Weiss 2002; Houghton & Bushby 2011), although there is evidence for similar states in earlier work on two-dimensional natural convection in a vertical slot (Ghorayeb & Mojtabi 1997). The existence and stability of these structures has elicited considerable interest in recent years (Knobloch 2008). Studies of model equations such as the Swift–Hohenberg equation and the use of branch-following techniques on the equations of fluid dynamics have revealed a close relationship between bistability and the presence of convectons (Burke & Knobloch 2007). Specifically, convectons are found in a region called the *pinning* or *snaking* region in parameter space inside the region of bistability between the conduction state and spatially periodic convection. In systems with one extended spatial dimension, the convectons appear in a (subcritical) primary bifurcation from the conduction state and do so simultaneously with periodic convection. Depending on the presence or absence of midplane reflection symmetry, there are either four or two families of localized states distinguished by their spatial phase ϕ (Burke & Knobloch 2007). Convectons with phase $\phi = 0, \pi$ are even under spatial reflection $x \to -x$ with either maxima ($\phi = 0$) or minima ($\phi = \pi$) at $x = 0$. Convectons with phase $\phi = \pi/2, 3\pi/2$ are odd

† Email address for correspondence: david.lojacono@imft.fr

under spatial reflection with either positive ($\phi = \pi/2$) or negative ($\phi = 3\pi/2$) slope at $x = 0$. Only even-parity states remain when midplane reflection is absent (Houghton & Knobloch 2011).

Despite its important role in identifying convectons, numerical continuation has not been applied to the equations of magnetoconvection. Existing attempts to explain the existence of convectons in these equations use matched asymptotic expansions valid in the limit of small diffusivity ratio ζ (Dawes 2007) or model equations in the spirit of the Swift–Hohenberg equation (Cox, Matthews & Pollicott 2004; Dawes 2008). In fact, the magnetoconvection problem differs in an important way from other systems exhibiting convectons. This is because of the presence of a conserved quantity, here the magnetic flux associated with the imposed vertical magnetic field (Matthews & Cox 2000). As anticipated by Cox & Matthews (2001) within weakly nonlinear analysis and subsequently by Dawes (2007) in his analysis of the $\zeta \to 0$ limit of the full magnetoconvection equations, this fact is responsible for two new features of the bifurcation diagram: (i) localized states exist *outside* the bistability region; and (ii) the resulting snaking diagram is *slanted*. In the analysis both these facts are a consequence of the presence of non-local terms in the amplitude equations, and these non-local terms are in turn a consequence of the presence of the conserved magnetic flux. Significantly, we also find that: (iii) slanted snaking and hence spatially localized structures are present even when the primary instability to a periodic state is supercritical and the region of bistability is absent. Dawes (2008) has constructed a one-dimensional model of the magnetoconvection equations, following Cox & Matthews (2001), which captures all three of these properties.

In this paper we use numerical continuation on the magnetoconvection equations in two dimensions to demonstrate that the conclusions reached by Dawes (2007, 2008) in his asymptotic analysis remain broadly correct for general parameter values. We show, moreover, that the system behaves fundamentally like other pattern-forming systems coupled to a conservation law (Dawes & Lilley 2010). However, we also demonstrate that the slanted snaking that results is a finite size effect, and relate the solutions along the slanted snaking branches to the modulated roll states first identified in the supercritical regime by Cox & Matthews (2001) by means of a weakly nonlinear multiscale analysis. Thus our work can be considered to be an extension of both approaches into a parameter regime where they overlap. This extension makes it possible in turn to relate the results of these two approaches to each other. In particular, by calculating the branches of strongly modulated rolls (hereafter referred to as localized states) and their stability properties, we shed additional light on the origin of the modulational instability of periodic convection in this system first noted by Cox and Matthews.

We conclude that in finite domains the mechanism responsible for snaking in this system is greatly modified by the non-local nature of the problem from the homoclinic snaking that lies behind localized structures in other fluid systems (Batiste *et al.* 2006; Bergeon & Knobloch 2008; Lo Jacono, Bergeon & Knobloch 2010; Schneider, Gibson & Burke 2010) and explain why the results are so sensitive to the spatial period used in the computations.

2. Basic equations

Two-dimensional magnetoconvection in an imposed vertical magnetic field is described by the dimensionless equations (Weiss 1981)

$$\nabla^2\psi_t + J(\psi, \nabla^2\psi) = \sigma R\theta_x + \sigma\zeta QJ(x + A, \nabla^2 A) + \sigma\nabla^4\psi, \tag{2.1}$$

$$\theta_t + J(\psi, \theta) = \psi_x + \nabla^2\theta, \tag{2.2}$$

$$A_t + J(\psi, A) = \psi_z + \zeta\nabla^2 A, \tag{2.3}$$

with ψ, θ and A defined such that the velocity $\boldsymbol{u} = \boldsymbol{\nabla} \times \psi\hat{\mathbf{y}}$, the temperature $T = 1 - z + \theta$ and the magnetic field perturbation $\mathbf{b} = \boldsymbol{\nabla} \times A\hat{\mathbf{y}}$. The system is characterized by four dimensionless parameters: the Rayleigh number $R \equiv g\alpha\Delta T h^3/\kappa\nu$, measuring the strength of the thermal forcing (i.e. the temperature difference ΔT across the layer); the Chandrasekhar number $Q \equiv B_0^2 h^2/\mu\rho_0\eta\nu$, measuring the strength of the imposed magnetic field B_0; and the two diffusivity ratios $\sigma = \nu/\kappa$ and $\zeta = \eta/\kappa$. Here α is the coefficient of thermal expansion, g is the gravitational acceleration, ρ_0 is the density at a reference temperature, ν is the kinematic viscosity, and κ and η are the thermal and ohmic diffusivities. The equations have been non-dimensionalized with respect to the thermal diffusion time h^2/κ in the vertical, where the length scale h refers to the layer height.

We study these equations with stress-free, fixed-temperature, force-free boundary conditions

$$\psi = \psi_{zz} = \theta = A_z = 0 \quad \text{on } z = 0, 1. \tag{2.4}$$

The resulting equations are considered on a horizontally periodic domain with dimensionless period Γ that is large compared with the critical wavelength λ_c of the (steady-state) convective instability that sets in as the Rayleigh number R is increased. With these boundary conditions, the equations are equivariant with respect to horizontal translations $x \to x + \ell$, $(\psi, \theta, A) \to (\psi, \theta, A)$, as well as the reflections R_1, R_2, where

$$R_1: \quad (x, z) \to (-x, z), \quad (\psi, \theta, A) \to (-\psi, \theta, -A) \tag{2.5}$$

relative to an arbitrary origin, here $x = 0$, and

$$R_2: \quad (x, z) \to (x, 1 - z), \quad (\psi, \theta, A) \to (-\psi, -\theta, A). \tag{2.6}$$

In addition $\bar{A} \equiv \Gamma^{-1}\int_0^\Gamma \int_0^1 A(x, z, t)\,\mathrm{d}x\,\mathrm{d}z$ remains constant in time. We solve (2.1)–(2.4) using a spectral element numerical continuation method (Assemat, Bergeon & Knobloch 2008; Bergeon & Knobloch 2008) with $\bar{A} = 0$.

Linear stability theory shows that the conduction state $(\psi, \theta, A) = (0, 0, 0)$ loses stability with respect to exponentially growing disturbances with wavenumber k when R reaches $R(k) = (p^3/k^2)[1 + (\pi^2/p^2)Q]$, where $p \equiv \pi^2 + k^2$. The critical Rayleigh number $R_c \equiv R(k_c)$ and the wavenumber k_c of the critical disturbance are obtained by minimizing the onset Rayleigh number with respect to k. Classical theory shows that at $R = R_c$ a steady-state bifurcation creates a branch of spatially periodic states with wavenumber k_c that bifurcates subcritically when

$$1 + \frac{\pi^2}{p^2}\left[1 + \frac{2\pi^2(p - 2\pi^2)}{p(p - \pi^2)}\frac{1}{\zeta^2}\right]Q < 0 \tag{2.7}$$

and supercritically otherwise (Knobloch, Weiss & Da Costa 1981; Weiss 1981). Moreover, when the condition (2.7) holds and the problem is formulated on the real line, this instability gives rise, in addition, to four subcritical branches of spatially localized states, characterized by their spatial phase $\phi = 0, \pi/2, \pi, 3\pi/2$ (Burke & Knobloch 2007). The states with $\phi = 0, \pi$ have even parity, i.e. they satisfy $R_1(\psi, \theta, A) = (\psi, \theta, A)$ and are related by R_2. Likewise, the states $\phi = \pi/2, 3\pi/2$ are of odd parity, i.e. they satisfy $R_2 \circ R_1(\psi, \theta, A) = (\psi, \theta, A)$ and are also related by R_2. We mention that in a periodic domain of finite period the branches of localized

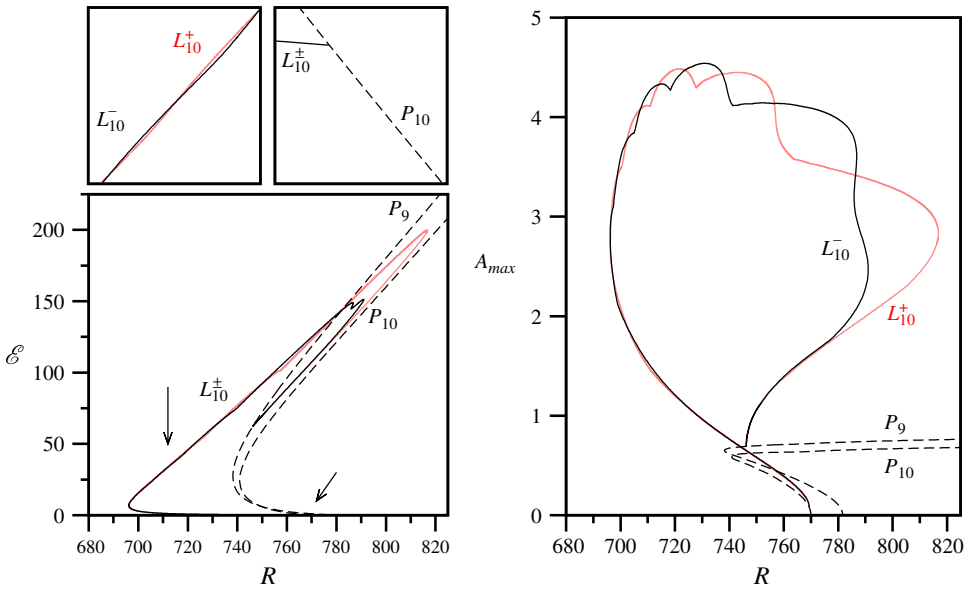

FIGURE 1. (Colour online available at journals.cambridge.org/flm) The convecton branches L^+ (red/grey in print) and L^- (black) together with the periodic states P_{10} and P_9 (dashed) when $\Gamma = 10\lambda_c$, $\zeta = 0.1$, shown in terms of the total kinetic energy $\mathscr{E}$ in the domain (left panels) and the maximum A_{max} of the potential $A(x, z)$ in the domain (right panel), both as functions of the Rayleigh number R. The insets at top left show enlargements at the locations indicated by arrows, and reveal that the convecton branches bifurcate together from the P_{10} branch and are intertwined at larger amplitude. This intertwining is shown more clearly in the right panel in terms of A_{max}. The convectons on the upper branch between the left and right saddle node bifurcations are stable.

states cannot bifurcate from the conduction state and necessarily bifurcate from the periodic states in a secondary bifurcation; this bifurcation occurs at small amplitude when $\Gamma \gg \lambda_c$.

The above properties of the system are shared with other doubly diffusive systems (Batiste *et al.* 2006; Lo Jacono *et al.* 2010) and are a consequence of the symmetry R_2 of (2.1)–(2.4) with respect to midplane reflection. However, when we initialize numerical continuation using analytically constructed approximations to the even and odd convectons and follow the resulting convecton branches, we find that the system behaves quite differently, as shown next.

3. Results

In this section we present results for $Q = 4$, $\sigma = 1$ and $\zeta = 0.1$ (subcritical case) and $\zeta = 0.5$ (supercritical case), and explore the role played by the aspect ratio Γ of the domain. For these parameter values $R_c \approx 769.98$, $k_c \approx 2.3948$, independently of the value of ζ, and overstability is absent. Thus the first bifurcation encountered as R increases is the steady-state bifurcation at $R = R_c$. We consider spatial periods $\Gamma = 10\lambda_c, 20\lambda_c, 40\lambda_c$, where $\lambda_c \equiv 2\pi/k_c$ is the basic wavelength of the unstable mode.

Figure 1 (left panels) shows the kinetic energy $\mathscr{E} \equiv (1/2)\int_0^\Gamma \int_0^1 |\boldsymbol{u}|^2 \,\mathrm{d}x\,\mathrm{d}z$ as a function of the Rayleigh number R for a pair of periodic states labelled P_{10} and P_9 (dashed lines), and a pair of spatially localized states of even (L^+, red line/grey

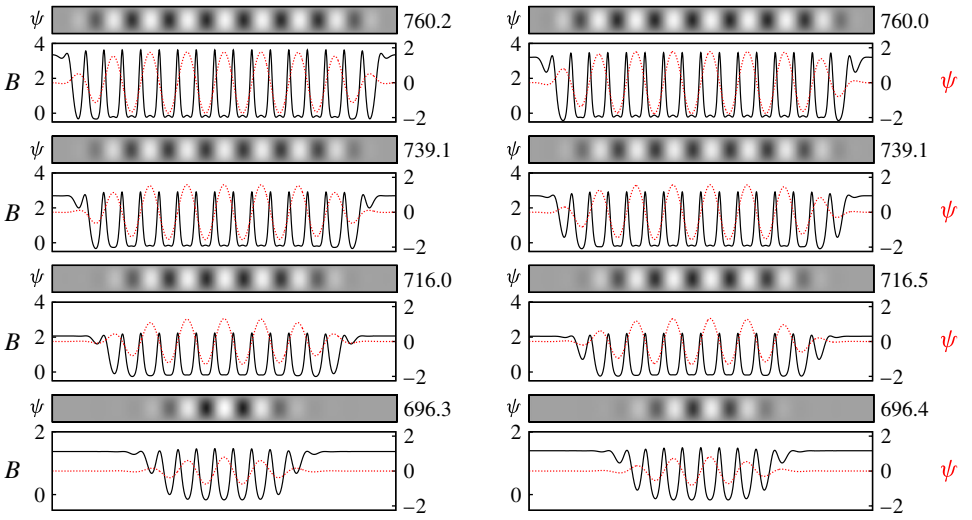

FIGURE 2. (Colour online) Solution profiles along the stable upper convecton branches L^+ (left column) and L^- (right column) in figure 1 at the Rayleigh numbers indicated on the right in terms of contours of the streamfunction ψ (upper panels) and the profiles of $\psi(x, 1/2)$ (red, dashed) and the resulting vertical magnetic field $B \equiv 1 + A_x(x, 1/2)$ (black, solid).

in print) and odd (L^-, black line) parity, both for $\zeta = 0.1$ and $\Gamma = 10\lambda_c$. This representation does not distinguish between states related by the midplane symmetry R_2 or by translations. The P_{10} state consists of 10 wavelengths (20 rolls) within the period Γ and hence bifurcates from the conduction state at R_c. Since ζ is small, this bifurcation is strongly subcritical, and, as predicted by general theory (Bergeon *et al.* 2008), is accompanied by two pairs of branches of opposite-parity spatially localized structures that bifurcate from P_{10} at small amplitude in a secondary bifurcation and do so together and likewise subcritically. These structures are initially weakly localized and unstable, and the resulting behaviour corresponds to the usual picture of the origin of localized states in systems of this type (Burke & Knobloch 2007). This is because for these small amplitudes the magnetic flux constraint exerts essentially no influence. It is this constraint, however, that is responsible for the subsequent behaviour of the localized states, and in particular for the fact that the localized branches extend to Rayleigh numbers substantially *below* not only the saddle node of P_{10} but in fact the saddle nodes of *all* the periodic branches bifurcating from the conduction state (figure 1). Thus localized states are present in a parameter regime with no coexistence between homogeneous and periodic states (Blanchflower 1999).

The localized states acquire stability via saddle node bifurcations ($R \approx 696.2$), where the branches turn around towards larger R and thereafter increase *monotonically* in energy as the length of the structure progressively increases. This is in contrast to systems exhibiting standard homoclinic snaking in which the nucleation of a new cell is reflected in the presence of a saddle node bifurcation in the bifurcation diagram. Figure 2 shows the details of this process, showing snapshots of both even- and odd-parity states of increasing energy. With increasing R both branches encounter a further saddle node at which they lose stability, and turn back towards smaller R before terminating together on a different periodic branch, P_9, with 18 rolls in the domain. Beyond this point the P_9 state is stable. Note that even and odd convectons

terminate in different (symmetry-related) P_9 representatives, as explained by Mercader *et al.* (2011).

During the growth process initiated near the left saddle nodes the midplane magnetic potential $A(x, z = 1/2)$ develops a negative slope within the structure, which remains almost constant despite the changing Rayleigh number and the growing number of rolls on either side. The rolls imprint a staircase structure on this overall slope, by an essentially kinematic flux expulsion process elucidated by Weiss (1966). Figure 2 shows the resulting vertical component of the magnetic field in the midplane, $B \equiv 1 + A_x(x, 1/2)$. The overall appearance of B is almost identical for both even and odd states. This is a consequence of the fact that the cells expel magnetic field regardless of their direction of rotation. Thus a churning array of cells expels field to the boundary of the array regardless of whether the outermost cells rotate in the same or opposite directions. Owing to the finite periodic domain, the expelled field raises the strength of the vertical magnetic field outside the structure, resulting in a vertical magnetic field that has an essentially piecewise constant profile when averaged over the cellular structure, reduced within the structure and enhanced outside, and largely independent of parity. The slanted convecton branches are therefore almost identical (albeit intertwined, a fact barely discernible when $\Gamma = 10\lambda_c$, figure 1). This is in contrast to binary fluid convection, where the pumping properties of a convecton depend strongly on its parity (Batiste *et al.* 2006). However, since the expelled magnetic field, whose magnitude depends only on the vigour of the cells and therefore on the imposed Rayleigh number, is redistributed over the domain outside of the convecton, the enhancement of the outside field depends inversely on $\Gamma - \ell_{convecton}$, where $\ell_{convecton}$ is the convecton length, and so vanishes in the limit $\Gamma \to \infty$, much as occurs in the corresponding binary convection problem (Mercader *et al.* 2009). This fact has important consequences, as we now describe.

Figure 3 shows that for larger values of Γ we start seeing the development of pairs of adjacent saddle nodes as the Rayleigh number increases. For moderate Γ these saddle nodes are associated with the filling of the domain and occur only after the localized structure has grown to almost fill the domain. Thus the saddle nodes on the branches of localized states are not associated with the growth mechanism of the localized structure. Indeed, for sufficiently small Γ the localized structure can grow gradually and monotonically in extent without undergoing any saddle node bifurcations whatsoever (figure 2) in a process dubbed 'smooth snaking' (Dawes & Lilley 2010). Thus the growth mechanism differs fundamentally from that associated with standard homoclinic snaking in a finite periodic domain (Burke & Knobloch 2007; Bergeon *et al.* 2008). The saddle nodes set in earlier and become more prominent for larger values of the aspect ratio Γ. Moreover, the slope that the branches make as a function of the Rayleigh number increases dramatically. Figure 4(*a*) shows that this increase is approximately linear in Γ, while figure 4(*b*) shows that, as Γ increases, the number of rolls in the structure at fixed Rayleigh number R also increases. Based on the results of figure 4 we conclude that this process continues indefinitely, implying that the slope continues to increase with increasing values of the period Γ becoming asymptotically vertical as in standard homoclinic snaking. During this process the even and odd localized states remain intertwined with the pairs of saddle nodes corresponding more and more closely to the insertion of a new pair of cells. However, for every finite Γ the slope remains finite and the snaking slanted. Consequently the presence of slanted snaking (Firth, Columbo & Scroggie 2007; Dawes 2008) is a finite size effect and one recovers the results from standard theory only in the limit $\Gamma \to \infty$. In this limit the magnetic field enhancement in the background vanishes (Mercader *et al.* 2009) and the

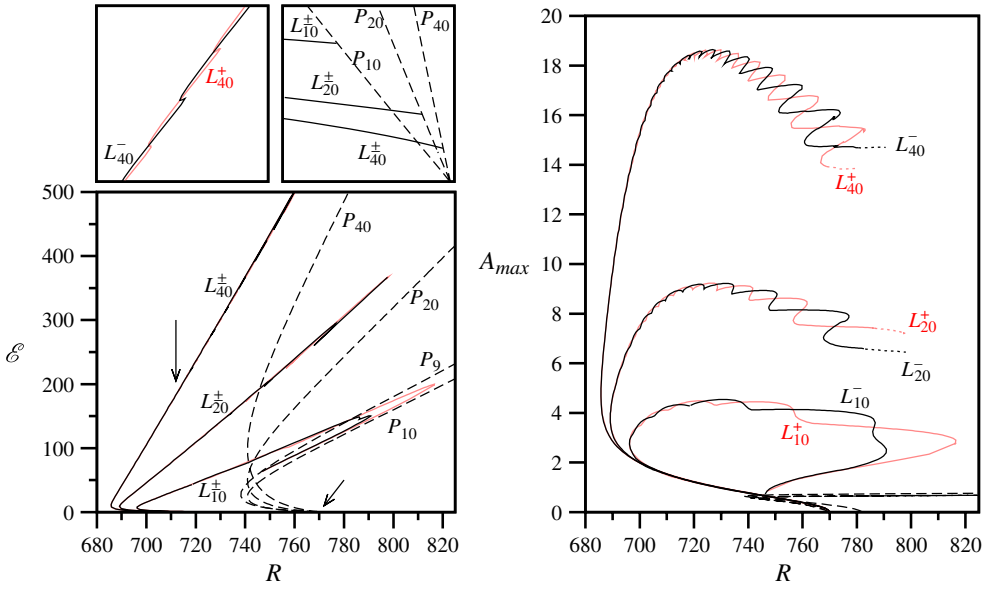

FIGURE 3. (Colour online) The convecton branches L^+ (red/grey in print) and L^- (black) together with the periodic states P_{10} (dashed) when $\Gamma = 10\lambda_c, 20\lambda_c, 40\lambda_c$, $\zeta = 0.1$, shown in terms of the total kinetic energy $\mathscr{E}$ in the domain (left panel) and the maximum A_{max} of the potential $A(x, z)$ in the domain (right panel), both as functions of the Rayleigh number R. The insets at top left show enlargements at the locations indicated by arrows, and reveal that with increasing Γ the convecton branches bifurcate from P_{10} at smaller and smaller amplitude and that they develop pairs of saddle node bifurcations but remain intertwined. This intertwining is shown more clearly in the right panel in terms of A_{max}. For $\Gamma = 20\lambda_c, 40\lambda_c$, only the initial part of the convecton branches is shown. In all cases the convectons on the upper branch between the left and right saddle node bifurcations are stable, except for the short intervals between successive saddle nodes.

saddle nodes align at R values corresponding to the first and last intersections between the unstable manifold of the conduction state (in *space*) and the corresponding centre-stable manifold of the periodic state (Woods & Champneys 1999).

In figure 5 we show the corresponding results for $\zeta = 0.5$. For this value of ζ all periodic branches bifurcate supercritically and existing theory (Burke & Knobloch 2007) shows that no localized states homoclinic to the conduction state as $x \to \pm\infty$ bifurcate from the conduction state at $R = R_c$. Instead one finds a pair of branches of solutions homoclinic to a *periodic* state that appear together with the periodic state (Iooss & Pérouème 1993; Dias & Iooss 1996). States of this type represent a defect in an otherwise uniform periodic state, and in a finite period domain bifurcate from the primary periodic branch in a secondary bifurcation as shown in figure 5. As a result the periodic state is stable close to R_c but loses stability almost immediately to perturbations with wavelength Γ. Figure 5 shows that this bifurcation in fact produces two defect states, of even and odd parity, both of which bifurcate subcritically from the periodic state and are therefore initially unstable. Further from this bifurcation the defect broadens and the defect states come to resemble the localized structures present in the subcritical case $\zeta = 0.1$, and both branches turn around towards larger R, again forming a large loop before terminating on a longer-wavelength periodic branch. Thus away from $R = R_c$ the localized states in the sub- and supercritical cases in fact behave

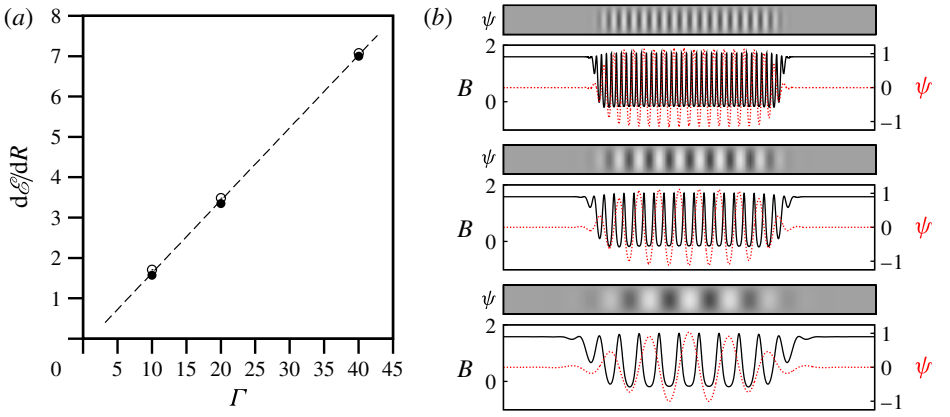

FIGURE 4. (Colour online) (*a*) The mean slope $\langle \mathrm{d}\mathscr{E}/\mathrm{d}R\rangle$ of the convecton branches as a function of the spatial period Γ when $\zeta = 0.1$ (solid circles) and $\zeta = 0.5$ (open circles). The slope is independent of ζ and is well fitted by the relation $\langle \mathrm{d}\mathscr{E}/\mathrm{d}R\rangle = 0.18(\Gamma - 0.35)$ (dashed line). (*b*) The convecton streamfunction (upper panels) and the profiles of $\psi(x, 1/2)$ (red, dashed) and $B \equiv 1 + A_x(x, 1/2)$ (black, solid) for $\Gamma = 10\lambda_c, 20\lambda_c, 40\lambda_c$ (from bottom to top) when $R = 700$. The solutions are plotted as a function of the scaled variable x/Γ. The convectons grow more and more rapidly in length as Γ increases.

in a very similar fashion (cf. figures 3 and 5) and with the *same* growth properties. The gradual steepening of the branches with increasing Γ follows the pattern already observed in the subcritical case, indicating the presence of finite size effects at any finite Γ. However, the pairs of saddle nodes on the solution branches now only appear for large values of Γ and are less prominent, suggesting that in the limit $\Gamma \to \infty$ the width of the snaking region may approach zero.

4. Discussion

It remains to understand the presence of localized states for parameters for which there is no bistability between conduction and convection. We have found two distinct cases where this occurs: in the subcritical case below the minimum of the saddle nodes of all the periodic states that bifurcate from the conduction state for $R \geqslant R_c$; and also in the supercritical case. We have seen that these states are in fact closely related and take the form of modulated rolls with a modulation scale that is comparable to the available domain. The appearance of this length scale in the problem is a consequence of the conserved quantity $\bar{A}$ or equivalently of a mean negative gradient of $A(x, 1/2)$ within the convecton, which must be balanced by a positive gradient outside if periodic boundary conditions are imposed. It is the resulting large horizontal scale of $A(x, 1/2)$ that is responsible for the ever-present finite size effects; these effects only disappear in an infinite domain in which the background gradient of $A(x, 1/2)$ vanishes and the non-local magnetic flux constraint formally drops out and the problem becomes local, with an intrinsic localization length. This distinction is an essential one: in a periodic domain a convecton is part of a periodic array of like convectons and the expulsion of flux from each of them raises the magnetic field between them. This is not the case in an infinite domain. This effect displaces the leftmost saddle nodes on $L^{\pm}$ towards larger Rayleigh numbers compared to the infinite domain, by an amount that decreases with increasing Γ as shown in figures 3 and 5. Since in small domains the saddle nodes of the periodic state and the convecton

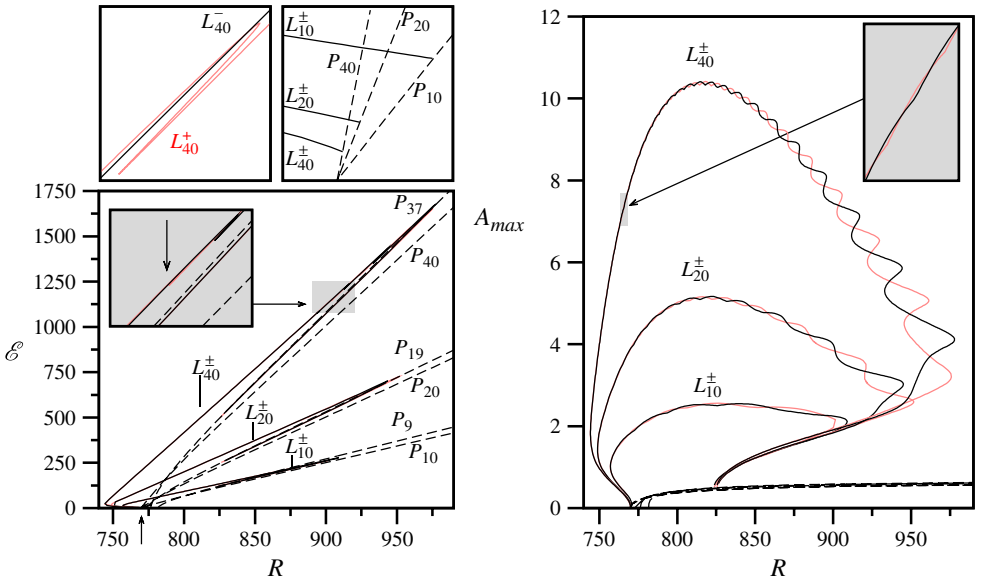

FIGURE 5. (Colour online) As for figure 3 but for $\zeta = 0.5$ and $\Gamma = 10\lambda_c, 20\lambda_c, 40\lambda_c$. The insets at top left show enlargements at the locations indicated by arrows, and reveal that with increasing Γ the convecton branches bifurcate from P_{10} at smaller and smaller amplitude and that they develop pairs of saddle node bifurcations. The right panel shows this behaviour in terms of A_{max}. In all cases the convectons on the upper branch between the left and right saddle node bifurcations are stable, except for the short intervals between successive saddle nodes.

states occur at comparable values of R, it follows that in large domains the saddle nodes of the latter necessarily fall substantially below the saddle node of the periodic state(s). Moreover the flux expulsion from the convecton reduces the magnetic field within the convecton and so enhances the vigour of the resulting motion and hence the kinetic energy $\mathscr{E}$. Thus the convection amplitude within the convecton exceeds that for periodic convection in which flux remains trapped between adjacent cells.

From figures 3 and 5 it is evident that in the limit $\Gamma \to \infty$ the left saddle nodes accumulate at a well-defined value of the Rayleigh number, $R^*(\zeta)$, with $R^*(\zeta = 0.1) \approx 690$ and $R^*(\zeta = 0.5) \approx 746$. Both values fall substantially below both R_c and the saddle nodes of the periodic states (if present). At R^* the mean slope $\langle \mathrm{d}\mathscr{E}/\mathrm{d}R \rangle$ of the intertwined $L^{\pm}$ branches diverges, as the localized states approach a spatially extended state of infinite energy, i.e. the solutions transition into a standard snaking scenario with no slant despite the absence of periodic states at this value of R^*. Figures 3 and 5 also show that at large amplitude the convecton branches track the P_{10} branch, suggesting that the solutions on the $L^{\pm}$ branches approach a spatially extended convection state with a defect. This defect collects the expelled magnetic flux, enhancing the kinetic energy of the asymptotic state over that of the corresponding P_{10} state. States of this type have been observed in other doubly diffusive systems as well (Bergeon & Knobloch 2008; Bergeon *et al.* 2008).

We can also understand the transition from the subcritical to the supercritical regime in the limit $\Gamma \to \infty$. As the parameter ζ increases, the periodic state bifurcates less and less subcritically but the bifurcation to localized states remains at R_c until the critical value $\zeta = \zeta^*(Q)$ at which the quantity (2.7) vanishes. At this point homoclinics

to the conduction solution turn into homoclinics to a periodic state (Dias & Iooss 1996). Nothing significant occurs elsewhere in the bifurcation diagram. Thus the broad features of the bifurcation diagrams are insensitive to the value of the parameters ζ and Q, provided overstability is absent, and indeed resemble those identified by Dawes & Lilley (2010) in their study of an oscillon model.

Our computational results confirm the basic conclusion of Cox & Matthews (2001) that the presence of the conserved flux $\bar{A}$ destabilizes periodic convection in the supercritical case, and the prediction by Dawes (2008) of slanted snaking in the subcritical case. These predictions were obtained on the basis of weakly nonlinear theory and a simplified model, respectively, but extend into the fully nonlinear regime, where neither procedure remains valid: in the former approach the solution amplitude and modulation length scale (i.e. domain length) are linked to the distance from threshold, while in the latter it is the inverse domain length that plays the role of the small parameter. In contrast, our calculations decouple the domain size from the Rayleigh number, allowing us to examine domains for which the scaling assumptions used in the theory no longer apply. This approach has allowed us to understand in detail the crossover from slanted snaking characteristic of finite domains to standard snaking on the real line.

This work was supported by the National Science Foundation under grant DMS-0908102 and by CNES under grant GdR MFA 2799.

REFERENCES

ASSEMAT, P., BERGEON, A. & KNOBLOCH, E. 2008 Spatially localized states in Marangoni convection in binary mixtures. *Fluid Dyn. Res.* **40**, 852–876.

BATISTE, O., KNOBLOCH, E., ALONSO, A. & MERCADER, I. 2006 Spatially localized binary fluid convection. *J. Fluid Mech.* **560**, 149–158.

BERGEON, A., BURKE, J., KNOBLOCH, E. & MERCADER, I. 2008 Eckhaus instability and homoclinic snaking. *Phys. Rev.* E **78**, 046201.

BERGEON, A. & KNOBLOCH, E. 2008 Spatially localized states in natural doubly diffusive convection. *Phys. Fluids* **20**, 034102.

BLANCHFLOWER, S. 1999 Magnetohydrodynamic convectons. *Phys. Lett.* A **261**, 74–81.

BLANCHFLOWER, S. & WEISS, N. 2002 Three-dimensional magnetohydrodynamic convectons. *Phys. Lett.* A **294**, 297–303.

BURKE, J. & KNOBLOCH, E. 2007 Homoclinic snaking: structure and stability. *Chaos* **17**, 037102.

COX, S. M. & MATTHEWS, P. C. 2001 New instabilities in two-dimensional rotating convection and magnetoconvection. *Physica* D **149**, 210–229.

COX, S. M., MATTHEWS, P. C. & POLLICOTT, S. L. 2004 Swift–Hohenberg model for magnetoconvection. *Phys. Rev.* E **69**, 066314.

DAWES, J. H. P. 2007 Localized convection cells in the presence of a vertical magnetic field. *J. Fluid Mech.* **570**, 385–406.

DAWES, J. H. P. 2008 Localized pattern formation with a large-scale mode: slanted snaking. *SIAM J. Appl. Dyn. Syst.* **7**, 186–206.

DAWES, J. H. P. & LILLEY, S. 2010 Localized states in a model of pattern formation in a vertically vibrated layer. *SIAM J. Appl. Dyn. Syst.* **9**, 238–260.

DIAS, F. & IOOSS, G. 1996 Capillary–gravity interfacial waves in infinite depth. *Eur. J. Mech.* (B/*Fluids*) **15**, 367–393.

FIRTH, W. J., COLUMBO, L. & SCROGGIE, A. J. 2007 Proposed resolution of theory-experiment discrepancy in homoclinic snaking. *Phys. Rev. Lett.* **99**, 104503.

GHORAYEB, K. & MOJTABI, A. 1997 Double diffusive convection in a vertical rectangular cavity. *Phys. Fluids* **9**, 2339–2348.

HOUGHTON, S. M. & BUSHBY, P. J. 2011 Localized plumes in three-dimensional compressible magnetoconvection. *Mon. Not. R. Astron. Soc.* **412**, 555–560.

HOUGHTON, S. M. & KNOBLOCH, E. 2011 The Swift–Hohenberg equation with broken cubic–quintic nonlinearity. *Phys. Rev.* E **84**, 016204.

IOOSS, G. & PÉROUÈME, M. C. 1993 Perturbed homoclinic solutions in reversible 1:1 resonance vector fields. *J. Differ. Equ.* **102**, 62–88.

KNOBLOCH, E. 2008 Spatially localized structures in dissipative systems: open problems. *Nonlinearity* **21**, T45–T60.

KNOBLOCH, E., WEISS, N. O. & DA COSTA, L. N. 1981 Oscillatory and steady convection in a magnetic field. *J. Fluid Mech.* **113**, 153–186.

LO JACONO, D., BERGEON, A. & KNOBLOCH, E. 2010 Spatially localized binary fluid convection in a porous medium. *Phys. Fluids* **22**, 073601.

MATTHEWS, P. C. & COX, S. M. 2000 Pattern formation with a conservation law. *Nonlinearity* **13**, 1293–1320.

MERCADER, I., BATISTE, O., ALONSO, A. & KNOBLOCH, E. 2009 Localized pinning states in closed containers: homoclinic snaking without bistability. *Phys. Rev.* E **80**, 025201(R).

MERCADER, I., BATISTE, O., ALONSO, A. & KNOBLOCH, E. 2011 Convectons, anticonvectons and multiconvectons in binary fluid convection. *J. Fluid Mech.* **667**, 586–606.

SCHNEIDER, T. M., GIBSON, J. F. & BURKE, J. 2010 Snakes and ladders: localized solutions of plane Couette flow. *Phys. Rev. Lett.* **104**, 104501.

WEISS, N. O. 1966 The expulsion of magnetic flux by eddies. *Proc. R. Soc.* A **293**, 310–328.

WEISS, N. O. 1981 Convection in an imposed magnetic field. Part 1. The development of nonlinear convection. *J. Fluid Mech.* **108**, 247–272.

WOODS, P. D. & CHAMPNEYS, A. R. 1999 Heteroclinic tangles and homoclinic snaking in the unfolding of a degenerate Hamiltonian–Hopf bifurcation. *Physica* D **129**, 147–170.